Chain Orientation in Polymer Networks: Computer Simulations Using the Bond Fluctuation Model

C. W. Yong[†] and P. G. Higgs*

School of Biological Sciences, University of Manchester, Oxford Road, Manchester M13 9PT, U.K.

Received October 29, 1998; Revised Manuscript Received March 1, 1999

ABSTRACT: Monte Carlo simulations of dense polymer networks under uniaxial strain were carried out using the three-dimensional bond fluctuation model. Particular attention is paid to the distribution of orientation for individual chain segments within the network and to comparison with experimental results from deuterium nuclear magnetic resonance (D-NMR). The simulated D-NMR spectrum has a split double-peak structure indicating that the segments have a degree of uniaxial orientation about the strain axis. The splitting disappears if the excluded volume restriction is removed from the simulation. This confirms that excluded volume and chain packing are important in determining orientational behavior. D-NMR spectra for dangling chain ends and for free chains within a network are also simulated and compared with experimental results. When the model dynamics is modified so that chains may pass through each other but the excluded volume restriction is maintained, it is found that the D-NMR spectrum is almost unchanged from the usual network. Thus, topological entanglements appear to have very little effect on the orientational behavior, at least for the relatively short chain lengths that we simulate here. The autocorrelation function for the uniaxial order parameter, $\langle P_2(\cos\theta)\rangle$, for each bond can be well-fitted by a stretched-exponential relaxation function. Relaxation times are almost constant along the majority of the chain but are significantly shorter within a few segments of free chain ends and significantly longer within a few segments of fixed chain ends. The apparent shapes of the D-NMR spectra are influenced by the total duration of the simulation, even when the simulation is several orders of magnitude longer than the orientational relaxation time of the chain segments. This observation is explained theoretically. Both experimental and simulated spectra have broad "wings" in addition to the central split peak. It is found that the spectrum for the chain middles and chain ends are very similar; i.e., segments close to chain ends do not contribute preferentially to the wings of the spectrum. It is found that chains with short end-to-end distances contribute principally to the central doublet of the full network spectrum. Segmental orientation in these chains is strongly influenced by excluded volume and chain packing and is insensitive to the end-to-end vector. Chains with long end-to-end distances contribute almost entirely to the wings of the full network spectrum, and segmental orientation is influenced principally by the chain end-to-end vector.

1. Introduction

Several experimental techniques such as fluorescence polarization,[1,2] optical dichroism,[3,4] and deuterium nuclear magnetic resonance (D-NMR)[5] have been used to study polymer networks at local or semilocal scales. From these studies it is generally agreed that there exist some kind of local correlations in the orientations of neighboring chains in strained polymeric networks. Orientation is also induced in probe molecules embedded in the network matrices because of coupling with the strained polymer chains. Probe molecules may be either small rigid molecules or free flexible chains.[6] D-NMR is one of the most informative methods to study orientation-dependent properties because of its ability to directly probe details at the molecular level through the deuterium quadrupole interaction.[5,7−13] In the case of elastomers, the behavior of different parts of the chain can be easily monitored by selectively introducing deuterium-labeled units.[9,10,12]

The classical phantom network theory explains rubber elasticity in terms of the reduction of chain entropy when a polymer network is strained.[14,15] The theory ignores interactions between chains and assumes that the only influence on the configuration of a chain is the position of its end points. The theory also makes predictions regarding chain orientation.[15,16] Segments in any chain have a tendency to align along the end-to-end vector of the chain. When a network is uniaxially deformed, the chain end-to-end vectors have a tendency to be aligned along the direction of strain. Hence, there is a net orientation of chain segments along the strain axis. The birefringence of a network is proportional to $\langle P_2(\cos\theta)\rangle$, where θ is the angle between the chain segment and the strain axis, P_2 is the second Legendre polynomial, and the average is taken over motions of each segment and over all segments. Phantom network theory predicts that birefringence is proportional to stress, and this is borne out by experimental results. D-NMR allows the distribution of $\langle P_2(\cos\theta)\rangle$ between segments to be measured rather than just the whole network average. The phantom network theory prediction for the D-NMR spectrum has been calculated by Sotta and Deloche[17] and is inconsistent with experimental observations. The theory predicts a single-peak spectrum that broadens as the strain is increased. The experiments show that the peak splits into a doublet and the magnitude of the splitting increases with strain.[9,10]

In a real network chains are closely packed, and these constraints restrict the freedom of motion and reorientation of chain segments and can lead to angular correlations between neighboring segments. Such effects

* To whom correspondence should be addressed.
[†] Present address: Department of Chemistry, University of Manchester, Manchester M13 9PL, U.K.

10.1021/ma981691a CCC: $18.00 © 1999 American Chemical Society
Published on Web 07/03/1999

are ignored in the phantom network theory. This was first raised by Di Marzio[18] who introduced an anisotropic interference due to excluded volume (EV) effects on a lattice model. Subsequent improvements or modifications of the model have also been reported.[19−21] Sotta and Deloche[17] introduced an anisotropic nematic-like mean field to take account of these local correlations in a deformed network. In this theory the D-NMR spectrum is split, since the mean field aligns the chain segments in a uniaxial way along the strain axis, while the influence of the chain end-to-end vector is less important. The theory is supported by several experimental observations. First, free chains diffusing in networks give a spectrum that has almost the same degree of splitting as for the network chains because of coupling between the free chains and network chains.[9,10] Second, the observed splitting varies in proportion to $P_2(\cos \Omega)$, where Ω is the angle between the strain axis and the magnetic field in the NMR experiment.[8,10] This is a strong indication of uniaxial segment distributions. Third, the degree of splitting observed for the short and long chains in bimodal networks is found to be equal.[22] Within the mean field theory this is understandable because short and long chains experience the same field,[22] whereas in the phantom network theory shorter chains would be more highly oriented because of the end-to-end vector effect.[15] Another theory by Brereton shows that excluded volume interactions lead to anisotropic screening between elongated chains[23,24] and also predicts a uniaxial character to the orientational distribution and a splitting of the NMR spectrum.

Computer simulations allow detailed investigations of molecular configurations that cannot be achieved by experimental means and are a useful link between theory and experiment. Monte Carlo simulations of polymer networks on a simple cubic lattice have been carried out by Depner et. al.,[25] who observed the splitting of the NMR spectrum and found that this varied with the strain in the way expected from the mean field theory. They also considered a free chain segment diffusing in the network and showed that the free segment had an induced anisotropy due to interaction with network chains. Using the same model, Sotta et al.[26] studied the way the NMR spectrum varied with chain density. Other polymer simulations using molecular dynamics[27,28] have considered chain orientation but not looked at the NMR spectrum.

In this work, we continue Monte Carlo simulations of polymer networks with specific reference to the D-NMR experiments. We use the three-dimensional bond fluctuation model (BFM)[29,30] for these simulations. This is an efficient type of simulation for dealing with many chains and has been used for a wide variety of applications including investigation of the polymer glass transition,[31] block copolymers and interfaces,[32] and polymer crystallization.[33]

In section 2 we describe the Monte Carlo (MC) chain model and simulation procedures. In section 3 we reproduce some of the results and show qualitative agreement with the experimental observations. Dynamics of chain orientation will be discussed in section 4, which include the observed features of the D-NMR spectra and the inherent statistical uncertainties in MC sampling. In the last section we consider the spectra of different parts of the chain separately and of different types of chains separately, and we investigate their contribution to the overall spectrum.

2. Simulation Model and Procedures

The BFM is essentially a cubic lattice model but with a wide spread distribution of bond vectors. The advantage of this model is that it is computationally much more efficient than free space because of the discrete lattice nature but at the same time mimics closely the properties of a more realistic free space model. Details of the model have already been given elsewhere.[30] Briefly, each monomer occupies a $2 \times 2 \times 2$ cube of sites on a cubic lattice. The monomers are connected to one another by a set of 108 allowed bond vectors that have a range of bond lengths between 2 and $(10)^{1/2}$ lattice units. Chains are self-avoiding; i.e., no part of any monomer may overlap any other monomer. The bond vectors are chosen such that the chain may not pass through each other. Hence, topological entanglements between chains can occur. We prefer to use this model rather than the simple cubic lattice model used in refs 25 and 26, since we are specifically interested in orientational behavior. The model allows a range of segment orientations that is much closer to an isotropic distribution than the three possible directions on a simple cubic lattice.

Simulations presented here use a total of 433 chains, each of length 40 monomers (39 segments) contained within a simulation box of size $44 \times 44 \times 110$ units. This gives a fraction of occupied sites of 0.65, which is well within the dense regime.[34] A high density is needed, since interchain interactions causing chain orientation act most strongly at high densities.[26] The simulation box has periodic boundary conditions, and the shape of the box was chosen to reflect the expected dimensions of an extended chain. The essential feature of a network is that the chain ends are localized in space. As a simple representation of the network, we will use a system of unconnected chains with fixed end points, as has also been used in refs 25−27. This is much simpler to set up than a fully connected network and avoids complications associated with network defects such as dangling ends and self-interacting chains.

The chains are initially generated as random walks in the box with no EV constraints. The system is then equilibrated using a "reptation" algorithm;[35] i.e., a monomer is removed from one end of a chain and replaced at the other end of the chain with a new bond vector chosen randomly. The resulting configuration is only accepted if no EV rule is violated. The move is repeated until a completely self-avoiding system is generated. The reptation movements reach an initial configuration for a dense system much more rapidly than the usual local moves of the BFM.[30] To generate a uniaxially extended network system, the choice of the new bond vectors during the reptation stage is biased as a function of $\cos \theta$. Once the initial configuration is generated, the ends of the chains are fixed in space and no longer permitted to move. During the simulation the internal monomers of the chains are moved using the usual single-step local moves permitted in the BFM: a randomly chosen monomer is moved by a single lattice site along one of the six possible directions, and the resulting configuration is only accepted if no EV rule is violated and if the new bond vectors generated belong to the allowed set. After the ends are fixed, the simulation is run for a further equilibration period in order to allow chains to reach a steady value of their mean square radius of gyration. After that, the sampling run is carried out. The system coordinates are recorded periodically at every 1.5×10^7 MC steps, which corresponds to about 9.1×10^2 attempted MC steps per moveable monomer (abbreviated as MCM). Typical simulations were for 2.34×10^{11} attempted MC steps or 1.42×10^7 MCM.

To estimate the value of the strain λ, we assume that the system is a set of affinely deformed chains. The mean square values of the three components of the chain end-to-end vectors are therefore

$$\langle R_i^2 \rangle = \frac{\langle R_i^2 \rangle_0}{\lambda}; \; i = x, y \qquad \langle R_z^2 \rangle = \lambda^2 \langle R_z^2 \rangle_0 \tag{1}$$

where the subscript 0 refers to the end-to-end components of

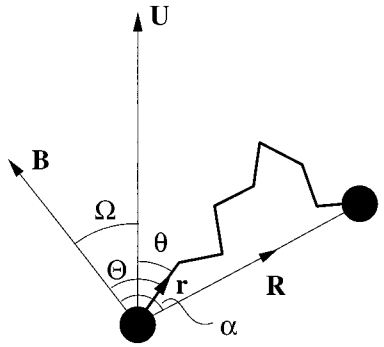

Figure 1. Orientation of a segment vector **r** with respect to various angular coordinates. Solid spheres represent the network junctions with end-to-end vector **R**. Vectors **B** and **U** represent the magnetic field and the direction of the uniaxial strain, respectively.

the system prior to deformation. We therefore define λ as

$$\lambda = \left[\frac{2\langle R_z^2\rangle}{\langle R_x^2\rangle + \langle R_y^2\rangle}\right]^{1/3} \quad (2)$$

For most of the simulations used here, the initial network configuration had the mean-square end-to-end components along *x*, *y*, and *z* directions of 22.73, 23.45, and 1194.1, respectively. This gives a value of $\lambda = 3.7$. This system forms a basis for reference for most of the paper; therefore, we call it system A. We also generated networks with $\lambda = 2.4$ and an isotropic network with $\lambda = 1$.

We will display results of the segment orientational distribution in a form that is directly comparable to the D-NMR spectra. The theory of NMR is outside the scope of the paper; we merely require the following results. For each monomer we measure the quantity $\Delta = \langle P_2(\cos(\Theta))\rangle$ where Θ is the angle between the chain segment and the direction of the magnetic field in the experiment, and the average is a time average over the whole simulation. In most cases we are considering a magnetic field parallel to the strain axis so that $\Theta = \theta$ and $\Omega = 0$ (see Figure 1). It is assumed that chain segment motion is rapid on the time scale of NMR measurement, in which case each chain segment is expected to give a pair of sharp peaks with a splitting proportional to Δ. The full network spectrum is the sum of contributions from each segment and can be written as $F(\Delta) = (^1/_2)[\rho(\Delta) + \rho(-\Delta)]$, where $\rho(\Delta)$ is the probability distribution of Δ values across all the network segments.[25,26] In practice we plot a histogram of Δ values using bins of width 0.005. For each segment we add 1 to the bins corresponding to $+\Delta$ and $-\Delta$. The final spectra are then normalized to give unit area under the curve.

3. Results: Factors Affecting the D NMR Spectrum

3.1. Effects of Strain and Magnetic Field Direction. We begin by demonstrating that the simulated spectra with the BFM simulation reproduce several of the features seen in the experimental spectra and in the previous simulations on the simple cubic lattice. It has previously been shown that chain segments close to fixed junction points have orientational behavior slightly different from those in the middle of chains.[12] This will be studied in detail below. Initially, however, we consider D-NMR spectra based on the contributions of all segments in chains, excluding the first three and last three segments at the ends of chains. Figure 2 shows calculated D-NMR spectra (with $\Omega = 0°$) of network systems with three values of λ. As expected from experimental results and the mean field theory (but not the phantom network theory), there is a single central peak for $\lambda = 1$, which splits into two as λ increases. In addition to the double peak, the spectra in Figure 2 also show broad "spectral wings" corresponding to segments having high Δ values when the network is stretched. The wings are characteristic of network spectra,[10,17] and we will discuss them further below.

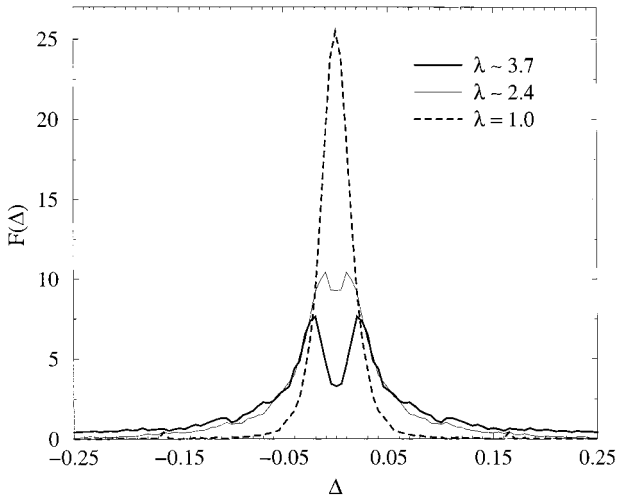

Figure 2. Calculated D-NMR spectra $F(\Delta)$ of chain systems with $\Omega = 0°$ and three values of λ.

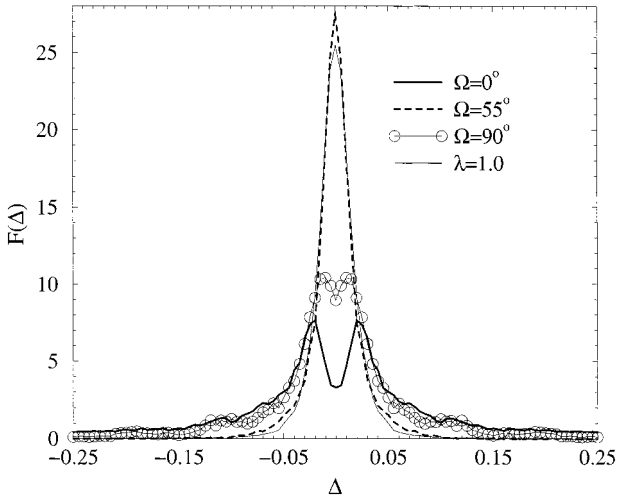

Figure 3. D-NMR spectra of the system A network with varying angle of the **B** field Ω. The splitting for $\Omega = 0°$ is roughly twice that for $\Omega = 90°$. For $\Omega = 55°$ no splitting is seen and the curve is almost indistinguishable from the curve for the relaxed system with $\lambda = 1.0$.

When the magnetic field angle Ω is varied, it is observed that the splitting of the experimental spectra follows closely the $|P_2(\cos\Omega)|$ dependence.[8,10,17] This is what would be expected if the segmental distribution were a simple uniaxial alignment along the strain axis. Figure 3 shows the D-NMR spectra of system A with different values of Ω. When $\Omega = 90°$, the magnitude of splitting is reduced approximately by half, and close to the magic angle, $\Omega = 55°$, the splitting is reduced to zero. Hence, the simulated spectra reproduce the observed behavior with Ω. Interestingly, at the magic angle the spectrum of the strained network ($\lambda = 3.7$) is almost identical to that of the unstrained network, which was also observed experimentally.[17] It should be noted, however, that the spectrum does not correspond merely to a simple uniaxial distribution. There is more information in the spectral shape than just the splitting

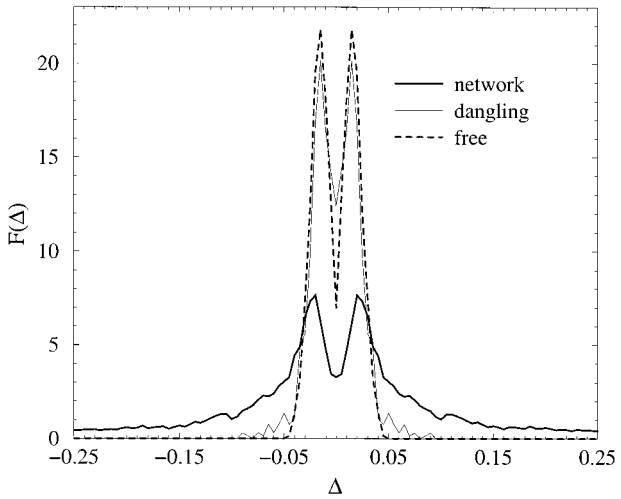

Figure 4. Comparison of the system A network D-NMR spectrum with those of free chains and dangling chains.

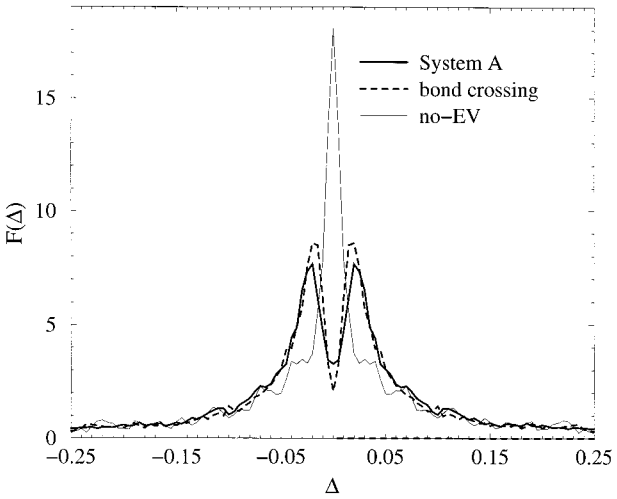

Figure 5. Comparison of D-NMR spectra at $\lambda = 3.7$ for system A (having both excluded volume and entanglements), a system with excluded volume but allowing bond crossing, and a system with no excluded volume.

of the central doublet. The wings of the spectra actually change shape with Ω rather than just getting proportionately broader or narrower. This indicates that segments are experiencing other types of constraints in addition to a mean-field-like effect along the strain axis.

3.2. Comparison of Network Chains, Dangling Chains, and Free Chains. As discussed in the Introduction, free chains diffusing in a network are often used as a probe of the orientational order of the network. We consider this case by randomly choosing 20 chains from the original system A and treating them as free chains where the ends are allowed to move in addition to the rest of the chain. In this way the density is still the same as system A and the network chains are as similar as possible to those in system A. We also consider a system with 20 chains treated as dangling ends with one fixed and one mobile end. Such chains are likely to exist in real networks, and it has been argued that they affect the shape of the NMR spectrum.[13,36]

In Figure 4 we show the D-NMR spectra of the free and the dangling chains compared with that of the network chains. In both cases there is a splitting that is of a similar order of magnitude to that of the network chains, indicating the presence of orientational coupling between the network and the free/dangling chains. Previous simulations with the simple cubic lattice[25] considered a single chain segment diffusing in the network as a probe and also showed the presence of orientational coupling, but free chain probes and dangling chains were not considered previously in simulations. It is also clear from Figure 4 that the wings of the spectra are absent for the free and the dangling chains. Once again, this is consistent with the experimental observation.[9,10] Our interpretation of this is that both free and dangling chains are able to relax their end-to-end vector, and hence, there will be no free and dangling chains that have an unusually large end-to-end distance. We show in section 5 that it is the highly extended chains in the network that contribute to the wings in the network spectrum.

The coupling coefficient ϵ is usually defined as a ratio of probe orientation over the network orientation. We find that the overall mean value of Δ for the network chain segments is 0.088 and for the free chains it is 0.018. This gives $\epsilon = 0.2$. Alternatively, if we define the ϵ in terms of ratio of the magnitude of splitting for the free and network chains, we obtain $\epsilon = 0.75$. The difference between the values obtained by the two definitions is due to the wings of the spectra. These increase the average Δ significantly for the network but not for the probe chain. Hence, the apparent coupling strength is small using the first definition. However, the splitting is very similar for both types of chain because they experience the same EV and packing constraints; hence, the coupling strength is larger using the second definition.

3.3. Excluded Volume and Entanglements. Orientational coupling between chains is clearly a result of EV interactions and will disappear in the absence of EV. We also know that the phantom network theory, which ignores EV interactions, predicts no overall splitting in the spectrum, even for large λ. We have tested this in a simulation that has no EV interactions (no-EV). In this case we use the same set of allowed bond vectors as usual, but the monomers are permitted to overlap. The ends of the chains are in the same positions as for system A; hence, the end-to-end vector distribution is the same. It is observed in Figure 5 that the no-EV spectrum has a single central peak with no splitting but that the wings of the spectra are very similar to system A; i.e., the overall spectrum is much broader than the isotropic network spectrum shown in Figure 2. This confirms that the EV interactions are required to give a splitting, as we expected, but shows that the deformation of the end-to-end vectors leads to a substantial broadening of the spectrum. This point is returned to in section 5.

We also considered the following two variants on the excluded volume interactions. First, we considered a case where excluded volume restrictions were applied to monomers within the same chain but not on different chains (within-chain EV) and, second, a case where excluded volume was applied between monomers on different chains but not on the same chain (between-chain EV). The within-chain EV spectrum (not shown) was very similar to the no-EV case. The between-chain EV spectrum had a slightly larger splitting than the usual system A spectrum and considerably more pronounced wings to the spectrum. Thus, it is the between-chain EV interactions that are responsible for the splitting, as expected.

Topological entanglements between chains arise as a result of the simple fact that chains cannot pass through one another. Entanglements constrain chain motion and reduce the entropy of network chains. Hence, entanglements should affect the entropic contribution to network elasticity. This has been modeled in a variety of ways using slip-links and tubes.[37,38] We would also expect that confinement of a chain in a tube would affect the freedom of chain segments to reorient and that this might show up as an effect on the shape of the NMR spectrum. By modification of the dynamics of the BFM, we can simulate a system that has no entanglements but that still possess excluded volume. This is achieved by allowing each attempted monomer movement to be either 1, 2, or 3 single lattice unit shifts in any of the lattice directions. For multistep moves each step is chosen in a different random direction. The move is accepted only if it satisfies the usual bond vector and EV constraints. In this way, configurations are the same as those of the BFM in all ways except that the chains may pass through one another.[30] There has been previous work based on BFM but using a different set of bond vectors, where it was shown that allowing crossing of polymer chains gave different dynamical behavior due to the absence of entanglements.[39] Here, the aim is to isolate the effects of entanglements of the orientational behavior from all other effects, and therefore, we wish to use exactly the same set of bond vectors so that there is no change to the static properties.

We see in Figure 5 that there is no significant difference in the spectra between the modified and the usual model in terms of both overall shapes and the splittings. Hence, entanglements appear to have little effect. However, entanglements will only matter if chains are longer than the entanglement length.[6] We might expect to see some effect if the chains were longer or if the density were higher, which would cause a reduction in the entanglement length. Previous estimates of the entanglement length in the bond fluctuation model[34] vary from 76 at density 0.3 (fraction of occupied sites) to 42 at density 0.5. We have not estimated the entanglement length for the density of 0.65, which we are using. Extrapolating these numbers might suggest a value around 30. This is not significantly shorter than the chain length of 40, which we are using. Therefore, this seems consistent with the interpretation that our chains are too short for significant entanglement effects. The present result nevertheless clearly shows that entanglements are not required in order to see a splitting in the NMR spectrum.

3.4. Test of Short-Range Orientational Correlations. The essence of the argument in the mean field theory for the D-NMR spectrum is that the constraints of packing segments together in a dense system lead to orientational correlations between neighboring segments. Although this local segment correlation is not directly observable in experiment, we can measure it directly in simulation. Consider two monomers separated by a distance r. For simplicity we consider only monomers with the same z coordinate; i.e., the vector connecting them lies in the xy plane. For each monomer, with the exception of the end monomers on chains, we define the direction of the chain to be the average of the two bond vectors that meet at that monomer. Let **u** be a unit vector in the direction of the chain at one monomer, let **v** be a similar unit vector for the other monomer, and let $\gamma_{u,v}$ be the angle between **u** and **v**.

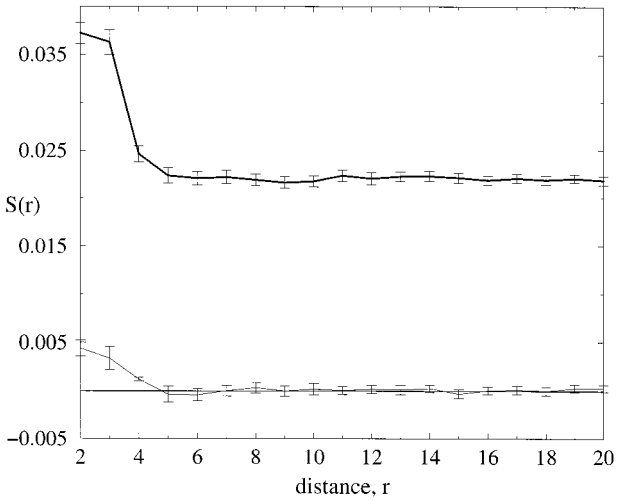

Figure 6. Pairwise correlation $S(r)$ in segment orientation as a function of distance between monomers calculated for $\lambda = 1.0$ (bottom curve) and $\lambda = 3.7$ (top curve).

The extent of local segment orientational correlation can be measured by the function

$$S(r) = \frac{\sum P_2(\cos \gamma_{u,v})}{N_r} \tag{3}$$

where the sum is over all pairs of monomers that have separation r in a set of instantaneous network configurations, and N_r is the number of pairs of monomers that have separation r. The fixed monomers at the ends of the chain are excluded from this sum. Figure 6 shows $S(r)$ for the strained network (system A) and the isotropic network ($\lambda = 1.0$). In the isotropic state there is a small positive local correlation extending over the range $2 \le r \le 4$ (note that r cannot be less than two lattice spacings because of excluded volume). There is no correlation at larger distances because there is no long-range order. In the case of the stretched network, $S(r)$ is nonzero at all distances because there is a net orientation of segments along the strain axis. There is an excess correlation at short distances that seems to extend to $r = 4$, as in the unstrained case.

4. Relaxation Dynamics of Chain Orientation

Here, we will study chain segment dynamics by looking at the autocorrelation function $C(t)$ of P_2 of each segment.

$$C(t) = \langle P_2[\cos \theta(t'+t)] P_2[\cos \theta(t')] \rangle - \langle P_2(\cos \theta) \rangle^2 \tag{4}$$

Since there are 40 monomers, we have 39 bonds per chain, which we label b_1 to b_{39}. Figure 7 shows the relaxation behavior for segments b_{19} in the middle of the chains and segments b_1 at the chain ends. Generally, segments that are close to fixed junctions relax most slowly and relaxation rates increase when moving toward the inner parts of the chains. To quantify this, two functional forms are used to fit the relaxation curves: the single-exponential form,

$$C(t) = A \exp(-t/\tau) \tag{5}$$

and the stretched-exponential form,

$$C(t) = A \exp[-(t/\tau_{st})^m] \tag{6}$$

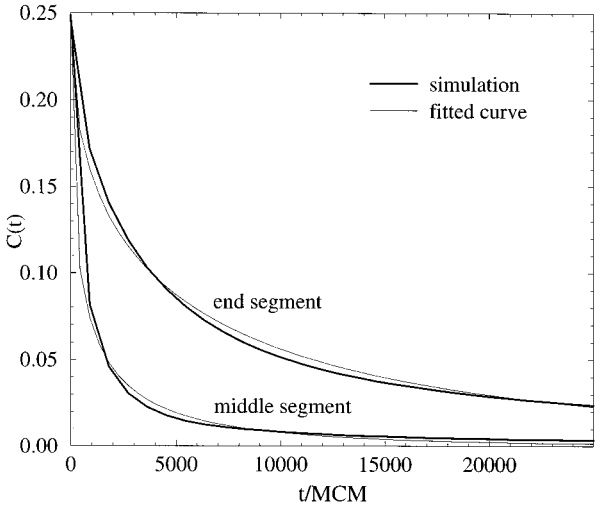

Figure 7. Time autocorrelation functions of segments in system A. The two bold lines are simulation data. The upper one is the mean $C(t)$ for the end segment b_1 averaged over all chains in the network, and the lower one is the mean $C(t)$ for the middle segment b_{19}. The thin solid lines are the best fits using the stretched-exponential function. Fits using the single exponential (not shown) are noticeably worse.

Table 1: Estimations of Parameters for Relaxation Curves $C(t)$ by Least-Squares Fitting for Various Polymer Systems[a]

model	segment	A	$\tau/10^3$ MCM	$\tau_{st}/10^3$ MCM	m
433 (all) network chains	b_1 (fixed end)	0.246	5.85	4.68	0.506
	b_2	0.249	1.68	1.00	0.388
	b_3	0.248	1.22	0.65	0.383
	b_4	0.249	1.11	0.58	0.391
	b_{19} (middle)	0.249	1.00	0.59	0.439
20 free chains (embedded in 413 network chains)	b_1 (free end)	0.243	0.54	0.36	0.607
	b_2	0.241	0.79	0.58	0.598
	b_3	0.240	0.87	0.61	0.551
	b_4	0.241	0.92	0.64	0.533
	b_{19} (middle)	0.239	0.94	0.61	0.489
20 dangling chains (embedded in 413 network chains)	b_1 (free end)	0.242	0.56	0.37	0.610
	b_2	0.240	0.79	0.58	0.605
	b_3	0.239	0.88	0.62	0.544
	b_4	0.240	0.91	0.62	0.526
	b_{19} (middle)	0.239	0.96	0.62	0.493
	b_{36}	0.243	1.02	0.64	0.467
	b_{37}	0.244	1.12	0.66	0.432
	b_{38}	0.244	1.54	0.96	0.418
	b_{39} (fixed end)	0.243	5.48	4.46	0.527

[a] See text for the definitions of the symbols.

where A is the value of $C(t=0)$, which can be measured directly, and the parameters τ, τ_{st}, and m are estimated by least-squares fitting of the data to the theoretical curve.

We have measured $C(t)$ for segments in network chains, free chains, and dangling chains as a function of the position of the segment along the chain. Table 1 lists parameter fittings of several segments in all of the chain systems. In the case of dangling chains, segments near both ends of chains are included because of the fact that the ends are not equivalent.

We found that single-exponential functions fit well to segments with the fastest rate of decorrelation. These segments are situated near extreme ends of chains with no junction constraints. However, the functions do not fit well to segments that are closest to junctions. On the other hand, the stretched-exponential forms fit well to all segments in all the systems, as shown in Figure 7. From Table 1 we see that the relaxation behavior is rather uniform along most of the chain except for segments within a few bonds from the chain ends. Moreover, the results also suggest that the free ends do not exert any noticeable influence on the fixed end or vice versa. This can be seen from the fact that the relaxation behavior of the segments near free ends (b_1 to b_{19}) in dangling chains is very similar to that of the corresponding segments in free chains. On the other hand, the relaxation behavior of the half of the dangling chain close to the fixed ends (b_{20} to b_{39}) is very similar to that of the corresponding segments in network chains (b_1 to b_{19}).

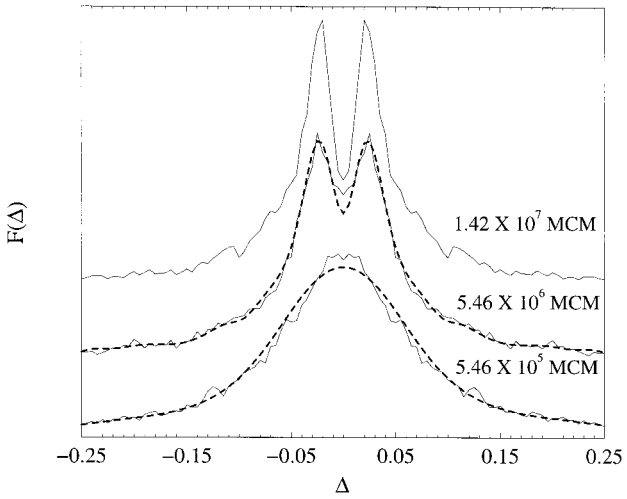

Figure 8. Three thin solid lines show the network spectra for system A averaged over 5.46×10^5, 5.46×10^6, and 1.42×10^7 MCM. The resolution of the doublet becomes increasingly sharp with increasing length of simulation. The bold dashed lines are the expected results for the two shorter times from eq 7. The curves have been shifted vertically for clarity. If the curves are not shifted, then the outer wings of all three spectra coincide almost exactly.

When plotting the NMR spectra, we are assuming that the segment motions are faster than the NMR time scale.[40−42] In the case of numerical simulations, a sufficient number of MC steps must be carried out in order to ensure adequate averaging over configurations accessible to each segment. In fact the apparent shape of the simulated NMR spectrum is sensitive to the total length of the simulation. Figure 8 shows the NMR spectra for system A obtained by taking the segmental orientations averaged over three different total lengths of the simulation: 5.46×10^5, 5.46×10^6, and 1.42×10^7 MCM, respectively. The results show that the doublet becomes more clearly resolved as the averaging time is increased. No doublet can be seen for the spectrum corresponding to the shortest time scale. The sensitivity of the results to the duration of the simulation is at first surprising, since the typical relaxation time of a segment is around 1×10^3 MCM from Table 1 so that even the shortest of these three averaging times is around 500 times longer than the relaxation time. We also note that the acceptance rate in the simulation is approximately 9% so that 10^3 MCM corresponds to 90 accepted moves per monomer.

The explanation is that the apparent shape of the spectrum is very sensitive to the statistical uncertainty in the estimation of the value of Δ for each segment. In the Appendix we consider the shape of the spectrum $F_{T_1}(\Delta)$ after averaging over a time T_1 (which is the longest time achievable in the simulation) and the same spectrum $F_{T_2}(\Delta)$ obtained after averaging over a shorter

time T_2. These spectral shapes are related by a convolution (denoted by *)

$$F_{T_2}(\Delta) = F_{T_1}(\Delta) * \frac{1}{\sqrt{2\pi{\sigma_0}^2/T_{\text{eff}}}} \exp\left[-\frac{\Delta^2 T_{\text{eff}}}{2{\sigma_0}^2}\right] \quad (7)$$

where σ_0^2 is a constant given in the Appendix and

$$T_{\text{eff}} = \frac{T_1 T_2}{T_1 - T_2}$$

In Figure 8 the broken lines indicate the shapes $F_{T_2}(\Delta)$, which are to be expected from eq 7 when $T_1 = 1.42 \times 10^7$ MCM and T_2 is each of the two shorter simulation times. The curves agree well with the measured spectra for these shorter times. The convolution limits the resolution that we can see in the simulation and causes the peak splitting to disappear altogether if the time is too short. In all the other spectra shown in this paper we always use the longest time averaging available, T_1, to estimate the spectra. This corresponds to roughly 1.4×10^4 times the typical segmental relaxation time. We checked that continuing simulation beyond this time would lead to very little further change in curve shape. The reason that the statistical error in the measurement of the Δ values has such a large effect is that the degree of orientation of most of the chain segments is actually very small. Each segment is exploring a wide range of orientations, and there is only a very slight bias of the average P_2 away from zero; hence, the fluctuation in P_2 for each segment is large compared to its mean. For further details see the Appendix.

The problem of resolution is important because it could lead to wrong conclusions about the shape of the spectrum. The problem arises in the simulations but has no equivalent in the experiments. We have nevertheless given a full treatment of the problem, since it will be a relevant issue in other polymer simulations. We note that the time between sampled configurations of the network was 9.1×10^2 MCM (see section 2), which is comparable to the typical segmental relaxation time. This corresponds to the most efficient sampling strategy. If configurations were sampled more frequently than this, they would not be independent of each other; hence, no new information would be gained. If configurations were sampled less frequently than this, then information would be wasted and the resolution would be worse.

5. Comparison of Orientational Behavior of Different Types of Chain Segment

Previous discussion of the shape of the D-NMR spectra has focused on the presence of the split doublet and the factors that affect the magnitude of the splitting.[6,9,10] Here, we consider the shape of the curve in more detail and determine which types of chain segment are contributing to the central doublet and the wings of the spectrum. It has been suggested that the different dynamical behavior of some types of segments is an explanation for the appearance of wing structrues.[8] It has also been argued that the wings may be a consequence of excess orientation of segments that are near network junctions.[12] We will show that in our results the wings arise from network chains that are particularly highly extended, that all segments on these highly extended chains contribute more or less equally, and that differences in dynamical behavior are not crucial for the wing shape.

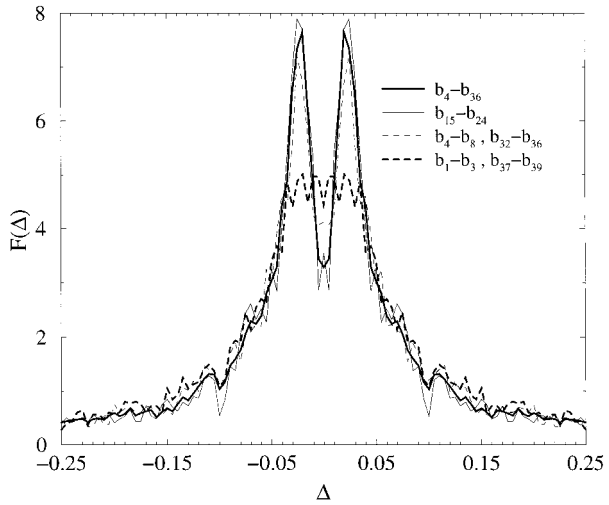

Figure 9. Calculated D-NMR spectra obtained from system A with $\Omega = 0°$. The various curves represent the spectra due to groups of segments derived from different parts of chain. The bold solid line represents all chain segments, excluding the first three and last three segments. The thin solid line represents middle portions of chains b_{15} to b_{24}. The thin dash line represent end portions of chains b_4 to b_8 and b_{32} to b_{36}. The bold dashed line represents extreme ends b_1 to b_3 and b_{37} to b_{39}. Only the extreme ends are significantly different because of poorer resolution in this case.

In Figure 9 we have calculated the D-NMR spectra from segments belonging to different parts of chains. It is seen that the spectrum is essentially the same for segments from all parts of the chain except for the few segments at the ends, for which there is apparently no splitting. However, the relaxation time for the end segments is longer, and therefore, the resolution is lower (see explanation in the Appendix). We believe that the absence of the doublet for the end segments is merely an artifact of the limited simulation time and that the spectrum for the end segments in the simulation would be almost the same as for the other segments if a longer simulation time were possible. In experimental systems the chemistry of the junctions themselves may cause additional effects that are not well modeled by the present simulation. In any case, the wings of the spectrum are the same for the end segments as the middle segments, even with the resolution that we have. Therefore, it is clear that the spectral wings are not associated with the ends of the chains.

To compare the effects of the chain end-to-end vector and the segmental packing constraints on the segment orientation, we separated the chains from the system A network into three different groups according to their end-to-end distance R. The three groups of chains, which we denote C_a, C_b, and C_c, have $R^2 \leq 500$, $501 \leq R^2 \leq 1500$, and $1501 \leq R^2$, respectively. The D-NMR spectrum for each group is shown in parts a−c of Figure 10. In the case of Figure 10a the narrow spectrum with doublet structure is clearly visible, which shows that it is the segments belonging to this group of chains that dominate the central part of the overall spectrum. Furthermore, the C_a spectrum has a shape that closely resembles that of the free chains and the dangling ends. The free chain spectrum is included in Figure 10a for comparison. This means that the effect of the junction position is not important here and that the segmental orientations are largely due to induced uniaxial order

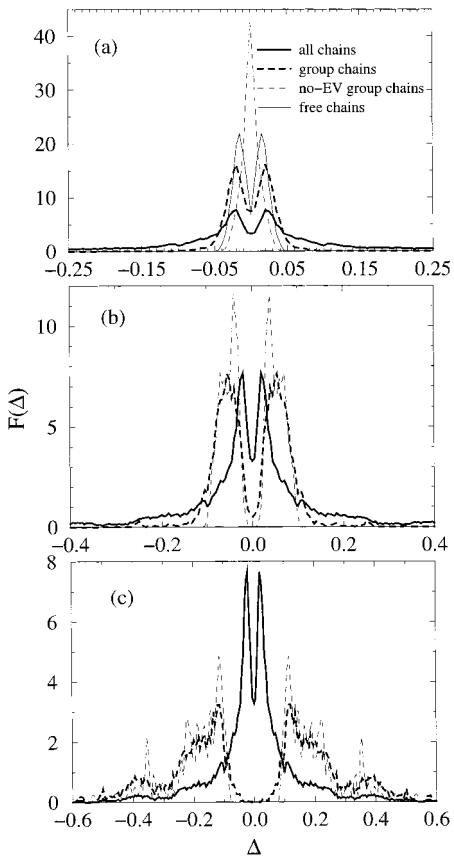

Figure 10. D-NMR spectra of different groups of chains in system A with $\Omega = 0°$: (a) group C_a chains; (b) group C_b chains; (c) group C_c chains. In each graph the bold solid line is the network spectrum for all chains, the bold dashed line is the spectrum for the chains in that group only, and the thin dashed line is the spectrum for that group of chains in the absence of EV interactions. In (a) the thin solid line is the spectrum of the free chains embedded in the network system (taken from Figure 4).

around the direction of strain. Also shown in Figure 10a is the spectrum for the C_a chains in absence of EV. This gives a single peak with no splitting; i.e., EV interactions between segments are required to produce the observed uniaxial order, as has been discussed earlier.

In the case of group C_b chains (Figure 10b) the apparent splitting is much larger than for the C_a chains, and for the C_c chains (Figure 10c) it is much larger again. For these two groups of chains the splitting still remains when the EV restrictions are removed. These chains are strongly influenced by the end-to-end vector because they are highly extended. Segments on highly extended chains tend to have large values of Δ even in the absence of the EV interactions. These segments contribute to the wing structure that we see in the overall spectrum. (Note that the apparent spikes for the no-EV spectrum in Figure 10c may be due to the discrete nature of the lattice, which is expected to be more important for highly extended chains, and due to the relatively small number of these chains, which leads to increased noise).

6. Discussion and Conclusions

These computational results are consistent with a large number of experimental observations and test several questions that cannot be looked at experimentally. The results extend previous simulation work by using the bond fluctuation model instead of the simple cubic lattice model, by using larger network sizes, and by looking at aspects that were not considered by simulation previously, including free chains and dangling chain ends, the effects of entanglements, and segment relaxation dynamics.

Taken together, these results seem to give a consistent picture of the orientational behavior of polymer networks under strain. It is clear that the split doublet observed in the NMR spectrum is a result of EV interactions between chains that introduce chain-packing constraints on the monomers and cause local short-range correlations in chain alignment, as shown in Figure 6. Stretching the network gives a preferred direction of alignment for these local correlations. Hence, the segments behave as though they were in a mean field oriented along the strain direction. Removal of the EV interactions leads to disappearance of the splitting in the simulations, confirming that the EV interactions are an essential requirement. The simulations also show that the behavior of the chain ends has little effect on the splitting in the spectrum, since network chains with fixed ends, dangling chains with one fixed end, and free chains all show doublet spectra. This is to be expected, since all these chains experience similar packing constraints. There had been a suggestion[13,36] that dangling chain ends in experimental networks were responsible in particular for the splitting in the spectrum. These results do not support this because the fixed network chains alone give a clearly resolved doublet in these results. The results also go some way toward justifying the simplified treatment of the network used here, which is really just a melt of chains with their ends fixed. If a real network of connected chains had been used, there would be some degree of fluctuation of the junction positions. However, we expect this would be largely irrelevant as far as the splitting of the NMR spectrum is concerned.

The work of Sotta and Deloche has tended to focus on just the magnitude of the NMR splitting as an indication of the state of the network and has emphasized the uniaxial nature of the orientational order. However, to understand the full shape of the spectrum, we must realize that the behavior of any one segment is influenced by both the end-to-end vector of the chain and the excluded volume interactions with other chains. In a network there will be chains with a range of end-to-end distances. Segments on chains that are highly extended have high degrees of orientation with respect to their end-to-end vector, and this results in a broad distribution of Δ values, as shown in Figure 10c. Almost all of the highly extended chains will have end-to-end vectors fairly closely aligned with the strain direction. Therefore, segments on these chains tend to have positive Δ, and there is almost no weight to the spectrum at the center. Elimination of the EV interactions makes very little difference to these chains, since it is the end-to-end vector of the chain that is the principal constraint. In contrast, for the group of chains C_a with short end-to-end distances, the position of the chain ends is a rather weak constraint. Segments in these chains experience constraints due to EV interaction with neighbors. This gives rise to a split doublet spectrum, Figure 10a, which is very similar to that of free chains or dangling chains that experience only the EV interactions and no chain end constraints.

In an experiment one cannot selectively label the most extended or the least extended chains as one can in a

simulation. However, similar information can be obtained by selectively labeling either the long or the short chains in a bimodal network. Chapellier et al.[22] emphasize that the observed splitting for short and long chains is almost the same and hence argue that the mean field effect due to chain packing and EV is more important than the effect of the end-to-end vector. Conversely, Gronski et al.[12] have argued that the distribution of lengths of elastically active chains in their networks is important. They show that for a given λ shorter chains are more oriented and have large values of Δ in the wings of the spectrum, whereas longer chains contribute to the center of the spectrum. This is understandable from the phantom network theory,[15] which shows that typical values Δ will be about $1/N$. Although we have not simulated bimodal or polydisperse networks, the picture emerging from our simulations suggests that both points of view are true. We expect that shorter chains will have larger values of Δ, and hence, the spectrum for short chains in a bimodal network should have broader wings than that for long chains. However, the splitting is caused by the behavior of chain segments on relatively extended chains, where the end-to-end vector is unimportant. Since EV interactions will be similar for all chains, it is likely that the degree of splitting will be similar for chains of different lengths.

The investigation of the relaxation dynamics of chain segment orientations that we carried out here was motivated by the observation that the apparent shape of the NMR spectrum was sensitive to duration of the simulation run, even for apparently very long simulations. Initially, we thought this indicated the presence of very slow relaxation processes in the segmental dynamics, or at least that a fraction of chain segments had very slow dynamics for some reason. Measurements of the autocorrelation functions $C(t)$ showed that segment dynamics was fast, with typical relaxation times of 10^3 MCM, which was much shorter than our simulation length. The mathematical analysis given in the Appendix showed that the reason for this was simply statistical uncertainty in the estimation of the mean orientational order for each segment, which occurs because the fluctuations in the order parameter are much larger than the mean. Using this theory, we were able to estimate the length of simulation required to get a reliable measure of the shape of the spectrum.

In fitting the relation functions, we simply used a phenomenological stretched-exponential form. We have not attempted a more in-depth analysis of chain dynamics (e.g., in terms of Rouse modes). This did not seem justified, since in a real network the connectivity of the chains and the fluctuation of junction point positions would have a significant influence on segment dynamics at this level of detail. One important point that the simulations do show is that the effects of chain ends on the dynamics extend only a very short distance from the ends (see Table 1). Only the first two or three chain segments from a free end or a fixed end differ significantly from the middle portion of the chain. This suggests that it is the surrounding medium of the other chains that is the principal influence on the chain segment dynamics at these short time scales.

By allowing bond crossing in the dynamics of the simulation, we showed that the entanglement effect does not seem to play an important role in influencing the orientation order for the chain length that we considered in this work. This does not rule out the possibility that entanglements will become significant for very long chains in the same way that for networks of very long chains the entanglement contribution to the entropic elasticity is likely to be larger than the contribution of the cross-links.[37] It may be possible to look at this in future simulation work. There is also room for further experimental work to look for possible effects of entanglements in chain orientation.

In this study of polymer network properties we have referred very closely to results from one type of experiment: D-NMR. This technique is extremely sensitive to distributions of chain properties and reveals subtle features that would not be seen by techniques that measure only average chain orientation. It appears that experiment, theory, and simulation are now coming together to give a detailed picture of the behavior of these materials.

Acknowledgment. This project is supported by the U.K. Engineering and Physical Sciences Research Council. We thank Paul Sotta and Bertrand Deloche for helpful and lengthy discussions of their work.

Appendix

Here, we estimate the effect that statistical uncertainty in measurement of the mean value of the orientational order for each bond will have on the apparent shape of the simulated NMR spectrum. During the simulation, configurations are stored at regular intervals $t = nt^*$, up to a total simulation length $T = Nt^*$. The mean value of the orientational order parameter for any one segment will therefore be

$$\Delta = \frac{1}{N}\sum_n P_2[\cos\theta(nt^*)] \tag{A1}$$

We expect that

$$\Delta = \Delta_0 + \delta \tag{A2}$$

where Δ_0 is the "true" value that would be obtained after an infinite simulation and δ is the statistical error from the finite sampling time of the simulation. The mean square statistical uncertainty is

$$\langle\delta^2\rangle = \frac{1}{N^2}\langle\sum_n\sum_m P_2[\cos\theta(nt^*)]P_2[\cos\theta(mt^*)]\rangle - \frac{1}{N^2}\langle\sum_n P_2[\cos\theta(nt^*)]\rangle^2$$

$$= \frac{1}{N^2}\sum_n\sum_m C(|n-m|t^*) \tag{A3}$$

We know that $C(t)$ is fitted well by the stretched-exponential function, eq 6. If the sampling interval t^* is small, we can replace the sum by an integral:

$$\langle\delta^2\rangle = \frac{1}{T^2}\int_0^T \mathrm{d}t_i \int_0^T \mathrm{d}t_j\, A \exp\left[-\left(\frac{|t_i - t_j|}{\tau_{st}}\right)^m\right]$$

$$= \frac{2A}{T^2}\int_0^T \mathrm{d}t_i \int_0^{t_i} \mathrm{d}t' \exp\left[-\left(\frac{t'}{\tau_{st}}\right)^m\right] \tag{A4}$$

Under the assumption that $T \gg \tau_{st}$ the integral can be evaluated approximately to give

$$\langle \delta^2 \rangle = {\sigma_0}^2/T \tag{A5}$$

where

$$ {\sigma_0}^2 = \frac{2A\tau_{st}}{m}\Gamma\left(\frac{1}{m}\right) \tag{A6}$$

and $\Gamma(x)$ is the gamma function. If the single-exponential fit to $C(t)$ had been used, we would have obtained the same result with $\sigma_0{}^2 = 2A\tau$.

There is thus a statistical uncertainty of

$$\frac{\pm\sigma_0}{\sqrt{T}}$$

in the measurement of Δ for each segment. Apart from segments close to the chain ends the correlation function is nearly the same for every segment. This is because the angular distribution of the segments is only very slightly biased from isotropic. For a completely isotropic segment where all 108 bond vectors of the BFM occur with equal probability, we have

$$A = C(0) = \frac{1}{108}\sum_i (P_2[\cos\,\theta_i)]^2 = 0.235 \tag{A7}$$

where θ_i is the angle of the ith bond vector of the BFM. This is very close to the measured values of A for the real segments. Fluctuations in Δ are thus of order $A^{1/2} = 0.48$, which is very much larger than the mean. Thus, to a good approximation $\langle \delta^2 \rangle$ is independent of Δ. Hence, the observed spectrum $F_T(\Delta)$ in a simulation of length T is related to the "true" spectrum $F_\infty(\Delta)$ by a convolution integral (denoted *).

$$F_T(\Delta) = F_\infty(\Delta) * \frac{1}{\sqrt{2\pi{\sigma_0}^2/T}} \exp\left[-\frac{\Delta^2 T}{2{\sigma_0}^2}\right] \tag{A8}$$

We cannot measure $F_\infty(\Delta)$, but we can measure $F_{T_1}(\Delta)$, corresponding to the longest simulation time, and $F_{T_2}(\Delta)$, corresponding to a shorter length simulation. From the properties of convolution integrals we obtain the relationship between these two functions given in the text (eq 7). For the results shown in Figure 8 we have estimated σ_0 from the stretched-exponential function, but if we use the single-exponential result, there is only a very small quantitative difference.

Note that the resolution of the $F_{T_1}(\Delta)$ function is

$$\frac{\sigma_0}{\sqrt{T_1}} = 0.007$$

which is roughly equal to the bin width of 0.005 used in the histogram. Increasing the time beyond this would make little difference to the shape of the curve. The resolution is also limited by the finite number of chain segments in the simulation; therefore, we cannot decrease the bin width indefinitely. In contrast, for the short simulation with $T_2 = 5.46 \times 10^5$ the resolution is

$$\frac{\sigma_0}{\sqrt{T_2}} = 0.037$$

which is large enough to significantly alter the apparent shape of the spectrum.

References and Notes

(1) Jarry, J. P.; Monnerie, L. *J. Polym. Sci.* **1980**, *18*, 1879.
(2) Erman, B.; Jarry, J. P.; Monnerie, L. *Polymer* **1987**, *28*, 727.
(3) Thulstrup, E. W.; Michl, J. *J. Am. Chem. Soc.* **1982**, *104*, 5594.
(4) Schmidt, P.; Schneider, B. *Makromol. Chem.* **1983**, *184*, 2075.
(5) Samulski, E. T. *Polymer* **1985**, *26*, 177.
(6) Ylitalo, C. M.; Zawada, J. A.; Fuller, G. G. *Polymer* **1992**, *33*, 2949.
(7) Deloche, B.; Samulski, E. T. *Macromolecules* **1981**, *14*, 575.
(8) Deloche, B.; Beltzung, M.; Herz, J. *J. Phys. Lett. (Paris)* **1982**, *43*, 763.
(9) Deloche, B.; Dubault, A.; Herz, J.; Lapp, A. *Europhys. Lett.* **1986**, *1*, 629.
(10) Sotta, P.; Deloche, B.; Herz, J.; Lapp, A.; Durand, D.; Rabadeux, J.-C. *Macromolecules* **1987**, *20*, 2769.
(11) Sotta, P.; Deloche, B.; Herz, J. *Polymer* **1988**, *29*, 1171.
(12) Gronski, W.; Stadler, R.; Jacobi, M. M. *Macromolecules* **1984**, *17*, 741.
(13) Kornfield, J. A.; Chung, G.-C.; Smith, S. D. *Macromolecules* **1992**, *25*, 4442.
(14) Flory, P. J. *Proc. R. Soc. A* **1976**, *351*, 351.
(15) Higgs, P. G.; Ball, R. C. *J. Phys. (France)* **1988**, *49*, 1785.
(16) Roe, R. J.; Krigbaum, W. R. *J. Appl. Phys.* **1964**, *35*, 2215.
(17) Sotta, P.; Deloche, B. *Macromolecules* **1990**, *23*, 1999.
(18) DiMarzio, E. A. *J. Chem. Phys.* **1962**, *36*, 1563.
(19) Tanaka, T.; Allen, G. *Macromolecules* **1977**, *10*, 426.
(20) Jarry, J. P.; Monnerie, L. *Macromolecules* **1979**, *12*, 316.
(21) Erman, B.; Bahar, I.; Kloczkowski, A.; Mark, J. E. *Macromolecules* **1990**, *23*, 5355.
(22) Chapellier, B.; Deloche, B.; Oeser, R. *J. Phys. II (France)* **1993**, *3*, 1619.
(23) Brereton, M. G. *Macromolecules* **1993**, *26*, 1152.
(24) Brereton, M. G.; Ries, M. E. *Macromolecules* **1996**, *29*, 2644.
(25) Depner, M.; Deloche, B.; Sotta, P. *Macromolecules* **1994**, *27*, 5192.
(26) Sotta, P.; Higgs, P. G.; Depner, M.; Deloche, B. *Macromolecules* **1995**, *28*, 7208.
(27) Gao, J.; Weiner, J. H. *Macromolecules* **1991**, *24*, 1519.
(28) Baljon, A. R. C.; Grest, G. S.; Witten, T. A. *Macromolecules* **1995**, *28*, 1835.
(29) Carmesin, I.; Kremer, K. *Macromolecules* **1988**, *21*, 2819.
(30) Deutsh, H. P.; Binder, K. *J. Chem. Phys.* **1991**, *94*, 2294.
(31) Binder, K.; Baschnagel, J.; Bohmer, S.; Paul, W. *Philos. Mag. B* **1998,** *77*, 591.
(32) Binder, K.; Muller, M.; Schmid, F.; Werner, A. *Physica A* **1998**, *249*, 293.
(33) Chen, C. M.; Higgs, P. G. *J. Chem. Phys.* **1998**, *108*, 4305.
(34) Paul, W.; Binder, K.; Heermann, D. W.; Kremer, K. *J. Phys. II (Paris)* **1991**, *1*, 37.
(35) Wolfgardt, M.; Baschnagel, J.; Binder, K. *J. Phys. II (Paris)* **1995**, *5*, 1035.
(36) Gronski, W.; Forster, F.; Pyckhout-Hintzen, W.; Springer, T. *Makromol. Chem., Macromol. Symp.* **1991**, *40*, 121.
(37) Higgs, P. G.; Ball, R. C. *Europhys. Lett.* **1998**, *8*, 357.
(38) Higgs, P. G.; Gaylord, R. J. *Polymer* **1990**, *31*, 70.
(39) Shaffer, J. S. *J. Chem. Phys.* **1995**, *103*, 761.
(40) Cohen-Addad, J. P.; Dupeyre, R. *Polymer* **1983**, *24*, 400.
(41) Sotta, P.; Deloche, B. *J. Chem. Phys* **1994**, *100*, 4591.
(42) Sotta, P.; Fülber, C.; Demco, D. E.; Blümich, B.; Spiess, H. W. *Macromolecules* **1996**, *29*, 6222.

MA981691A